Polymer 320 (2025) 128096

Contents lists available at ScienceDirect

Polymer

journal homepage: www.elsevier.com/locate/polymer

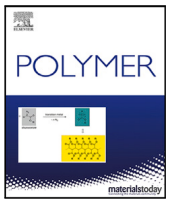

Low-density polyamide 12 foams using Bayesian optimization and inverse design

Karim Ali Shah [a], Rodrigo Q. Albuquerque [a,b], Christian Brütting [a], Marcel Dippold [a], Holger Ruckdäschel [a,b,c,*]

[a] University of Bayreuth, Universitätsstrasse 30, Bayreuth 95447, Germany
[b] Neue Materialien Bayreuth GmbH, Gottlieb-Keim-Strasse 60, Bayreuth 95448, Germany
[c] Bavarian Polymer Institute and Bayreuth Institute of Macromolecular Research, Universitätsstrasse 30, Bayreuth 95447, Germany

ARTICLE INFO

Keywords:
Bead foams
Polyamide 12
Batch foaming
Machine learning
Bayesian optimization
Active learning
Inverse design

ABSTRACT

This study introduces a novel, comprehensive approach to optimizing and designing batch foaming of low-density polyamide 12 (PA-12) using advanced machine learning (ML) techniques. Bayesian optimization was used to minimize the foam density, which decreased from approximately 900 to 150 kg/m^3 in a single new experiment. A PA-12 foam density of 50 kg/m^3, the lowest achieved, was recorded. In addition, an inverse design approach was used to check the robustness of the model by identifying the specific processing parameters required to achieve the desired foam density. Finally, PA-12 foams with similar densities but different processing parameters were obtained using ML. The study highlights the effectiveness of integrating these ML methodologies in the development of lightweight, high-performance polymer foams, which is much more sustainable than traditional methods for achieving low-density foams.

1. Introduction

Polymer-based materials have played a significant role in everyday life since their introduction in the early 20th century, shaping a wide range of industries and applications [1,2]. Over the decades, polymers have become integral to a vast range of applications, from packaging and insulation to key roles in the automotive and aviation sectors [3–7]. Their versatility also extends to the medical field, where different types of polymers are tailored for specific uses, such as in implants, drug delivery systems, and prosthetics [8–13].

Polymer foams are lightweight and insulating materials used in cushioning, thermal insulation, and acoustic damping, making them essential in consumer goods and industrial applications [14–16]. Polymer bead foams, with their unique bead structure, offer low-density foams with complex geometries, making them ideal for applications like protective packaging, automotive components, and lightweight construction materials. Since BASF introduced expandable polystyrene (EPS) in 1950, bead foams based on polymers like polypropylene (PP) and thermoplastic polyurethane (TPU) have been developed to meet diverse industry needs. Expanded TPU (ETPU) bead foams are popular in running shoe midsoles, while expanded Polyether block amide (EPEBA) bead foams are gaining attention for their lightweight and strong properties [17–24].

The demand for lightweight, high-performance materials in various industries has led to increased interest in the development of advanced foaming technologies. Polyamide (PA) bead foaming is one such, offering significant advantages in terms of material properties and application versatility. Expanded Polyamide 12 (ePA) bead foams have gained significant attention across various industries, particularly in the automotive sector, due to their light weight, low-density structure and exceptional thermo-mechanical properties [25]. Unlike more basic polymer foams like PS, PP, and PU, PA 12 offers superior mechanical strength, chemical resistance, and thermal stability, making it perfect for high-performance automotive applications. These high-performance characteristics are essential for components that must withstand harsh environments and high stress, such as seat cushions, interior panels, and other lightweight, high-strength parts that contribute to improved fuel efficiency and overall vehicle performance [26]. Additionally, ePA foams are extensively utilized in cold chain logistics, product packaging, and sports protection, construction materials, and consumer products, where their insulation, impact absorption, and durability are highly valued. The ongoing development of ePA bead foams continues to enhance their properties, broadening their applications across numerous sectors.

* Corresponding author at: University of Bayreuth, Universitätsstrasse 30, Bayreuth 95447, Germany.
E-mail addresses: holger.ruckdaeschel@uni-bayreuth.de, ruckdaeschel@uni-bayreuth.de (H. Ruckdäschel).
URL: https://www.polymer-engineering.de/ (H. Ruckdäschel).

https://doi.org/10.1016/j.polymer.2025.128096
Received 17 October 2024; Received in revised form 17 January 2025; Accepted 27 January 2025
Available online 3 February 2025

Artificial Intelligence (AI) has emerges as a powerful catalyst for change across multiple industries, reshaping how industries, businesses address complex challenges. The application of AI is vast, ranging from enhancing decision-making processes to automating routine tasks driving unprecedented efficiency, innovation, and competitive advantage. Its capabilities span diverse domains, including predictive analytics in finance, tailored marketing strategies in retail, autonomous technologies in transportation, and precision medicine in healthcare [27,28]. As AI continues to evolve, its impact on industries is expanding, enabling smarter, more adaptive systems that learn and improve over time. Within this broader AI landscape, machine learning (ML) and advanced optimization algorithms have become critical tools, revolutionizing how industries address specific challenges. The integration of ML and optimization is transforming traditional material science, enabling rapid prototyping, enhanced product performance, and greater adaptability to industry-specific needs. The polymer industry, in particular, has experienced a significant shift in material development and manufacturing. These technologies are especially valuable in creating lightweight, high-performance materials, where precision and innovation are essential.

ML enables engineers and scientists to analyze extensive datasets, identify patterns, and accurately predict material behavior under various conditions and processing parameters. This capability facilitates the design of superior materials with properties tailored to specific applications. Meanwhile, advanced optimization algorithms fine-tune manufacturing processes to ensure these materials meet the highest performance standards while minimizing waste and reducing production costs. Expanding the application of ML will be crucial for driving sustainability and contributing to a more sustainable world [29,30]. In recent years, ML has become increasingly prevalent in polymer bead foaming research, focusing on predicting key properties such as density, viscosity, and pressure [31,32]. Predictive models in this area are actively being developed and refined to optimize bead foaming processes [33,34]. Advanced optimization algorithms, such as Bayesian optimization (BO), have gained importance for identifying optimal solutions in various polymer processes. BO has proven effective in significantly reducing the time required to determine the best parameters for a wide range of applications. Its use has expanded to material formulation, where it optimizes specific properties [35–38]. For instance, Albuquerque et al. applied BO to maximize the glass-transition temperature (T_g) in an epoxy resin system composed of one resin and seven amino acid curing agents with stoichiometric ratios (R) of one-to-one. Remarkably, T_g reached its highest value after conducting only nine additional experiments. BO has also been effectively utilized in foaming processes to minimize experimental trials. Endres et al. demonstrated that BO-guided experiments significantly reduced the number of trials needed to achieve desired properties. Their study explored how variations in copolymer composition and the molar mass of styrene and methyl methacrylate copolymers influence key properties, such as foamability [39]. Optimizing foaming processes, particularly to achieve low-density foams, remains a complex challenge requiring the precise tuning of parameters such as pressure, temperature, and saturation time.

The objective of this paper is to address the challenges of achieving low-density PA 12 batch foaming while minimizing the number of experimental trials. To this end, BO was employed to generate initial trial suggestions. To account for uncertainties in the process, BO will also recommend an Active Learning (AL) point for further refinement. After each experiment, the measured density will be incorporated into the optimization process, enabling BO to suggest the next set of trials. This iterative approach will continue until the desired low-density foam is achieved. Once the optimal density is reached, inverse design technique was used to identify the processing parameters required to achieve a specific target density.

Table 1
Overview of autoclave processing parameters.

Parameter	Units	Min	Max
Pressure	Bar	60	200
Temperature	°C	20	300
Residence time	min	10	60

2. Materials and methods

2.1. Material

For this study, Polyamide 12 (VESTAMID® LX 9012), supplied by Evonik GmbH (Essen, Germany) was used. The material has a melting peak of 179.8 °C.

2.2. Autoclave bead foaming

Autoclave technology is extensively employed in the production of cellular structures made from thermoplastic polymers. In this study, batch foaming under pressure was conducted using a high-pressure autoclave equipped with temperature and pressure control units. The materials were placed inside the autoclave and carbon dioxide CO_2 was dosed in its supercritical state. After the desired saturation period, foaming was initiated by fully opening the release valve. The experiments systematically varied saturation time, pressure, and temperature to identify the optimal parameters for each material. An overview of these parameters is presented in Table 1, with further details available in [40]. A schematic representation of the autoclave setup is shown in Fig. 1.

2.3. Density measurement

The density of the PA 12 bead foams was determined using the Archimedes principle with a precision density balance [41]. Measurements were taken shortly after removing the beads from the autoclave, with the reported density representing the average of three samples. To assess material stability, density was also measured after 24 h, with no significant changes observed. The measurements were performed by weighing the samples in air and then submerged in water, and the density was calculated using the following equation:

$$\rho = \frac{A}{A - B} \times \rho_{\text{water}} \tag{1}$$

where:

- ρ is the density of the polymer foam,
- A is the sample's weight measured in air,
- B is the apparent sample's weight when submerged in water (buoyancy),
- ρ_{water} is the water density at the measurement temperature.

2.4. Morphology

The foam structure and morphology of the PA 12 beads were examined using a scanning electron microscope (SEM), JEOL JSM 6510. The beads were sectioned along their diameter and applying a thin gold coating through sputtering, and their cell morphology was analyzed using ImageJ software. For the analysis of each sample, at least 100 cells were evaluated to ensure the quality of the data. Additionally, the cell density, representing the number of cells per unit volume, was calculated based on a two-dimensional SEM image [40]. The cell density (N_0), representing the number of cells per unit volume in the foamed sample, was calculated using Eq. (2). This was determined based on measurements from a two-dimensional SEM image (Fig. 9).

$$N_0 = E.(nA)^{3/2} \tag{2}$$

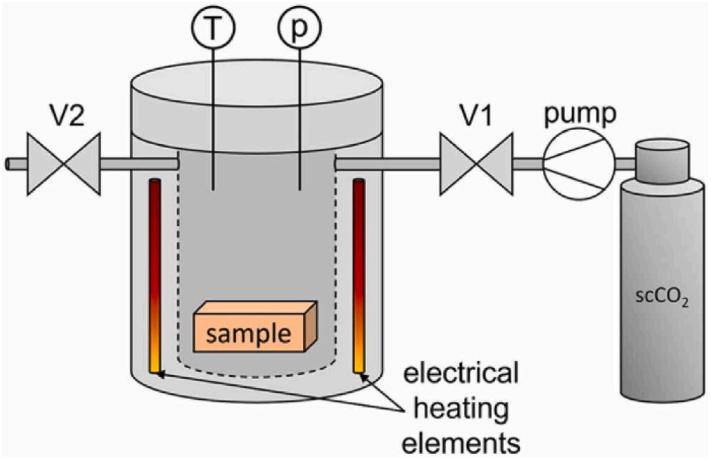

Fig. 1. Schematic representation of the autoclave setup, including the inlet and outlet valves (V1 and V2) and the electrical heating elements. *Source:* Reproduced with permission from Ref. [40].

In this equation, E is the expansion ratio, n refers to the number of identified cells, and A represents the total area occupied by these cells. This nucleation density combines the cell density (N_0) with the bulk polymer density ($\rho_{polymer}$) and the density of the foamed sample (ρ_{foam}), indicating the number of nuclei per unit volume in the unfoamed material prior to cell expansion. This approach provided insights into the foamed sample's structure.

2.5. Framework of Bayesian optimization and active learning

Bayesian Optimization (BO) is a probabilistic model-driven optimization method employed to identify the minimum or maximum values of a function. It is particularly useful for optimizing complex situations where each evaluation is costly and time consuming, such as parameter optimization in material science experiments. For example autoclave foaming. BO uses a surrogate model to approximate the objective function. Commonly, Gaussian Processes (GPs) are employed due to their ability to provide not only predictions but also uncertainty estimates. BO starts with an initial set of data points and fits a GP model. It then utilizes the acquisition function to determine the next point for evaluation. For each new point, the model is refined, and this iterative process continues until convergence is achieved. The surrogate model used in the BO runs was Gaussian Processes (GP), which is the best model known to date for this kind of optimization, as its predictions come automatically with the corresponding uncertainties, which are used inside the acquisition function employed during BO, as well as because it has a good performance for small datasets.

A GP is defined by a mean function $m(x)$ and a covariance function (kernel) $k(x, x')$. The mean function is specified as:

$$m(x) = \mathbb{E}[f(x)] \tag{3}$$

This is the expected value of the function $f(x)$ at the input x, before observing any data, here $\mathbb{E}$ represents the expected value or mean of a random variable.

For inputs x and x', the covariance is given by:

$$k(x, x') = \sigma^2 \exp\left(-\frac{(x - x')^2}{2\ell^2}\right) \tag{4}$$

where σ^2 is the variance and ℓ is the length scale.

The acquisition function directs the choice of the next evaluation point by balancing exploration (searching in areas with high uncertainty) and exploitation (focusing on areas likely to yield better optimization). Typical acquisition functions include Expected Improvement (EI) and Upper Confidence Bound (UCB). The Expected Improvement (EI) is calculated as:

$$\mathrm{EI}(x) = \mathbb{E}\left[\max\left(0, f(x^*) - f(x)\right)\right] \tag{5}$$

where $f(x^*)$ is the best observed value so far.

Active Learning (AL) is a technique used to selectively choose the most informative data points to label or evaluate, minimizing the number of experiments needed. In the context of BO, AL helps by selecting new candidate points based on the current model's uncertainty. The BO process includes AL component where the acquisition function not only aims to improve the objective function but also considers the uncertainty of predictions. AL helps the model queries the data points about which it is most uncertain. This uncertainty can be quantified by measures such as variance or entropy in probabilistic models. BO uses a surrogate model to predict outcomes and an acquisition function to suggest new evaluation points. AL refines this process by selecting points with high uncertainty or potential for significant improvement. Workflow of framework is as bellow,

1. Initialize with a set of sample points.
2. Fit a Gaussian Process model to these points.
3. Utilize an acquisition function to determine the next point for evaluation.
4. Apply Active Learning to address areas with high uncertainty.
5. Update the model with new data and repeat the process until the optimization converges.

2.6. Machine learning models

After completing the BO process, a dataset was generated for subsequent analysis. Different ML models were subsequently applied to the dataset to determine the most effective one. The models considered include Linear Regression (LR), Decision Trees (DT), Random Forest (RF), Gradient Boosting Regression (GBR), Gaussian Processes (GP), Lasso Regression (LASSO), Stochastic Gradient Descent Regression (SGDR), and Ridge Regression (RR). For the general description about the model please see [31,42]. Each model was assessed on its capacity to predict the target accurately and efficiently across various experimental scenarios. This involved comparing the models' performance in terms of prediction accuracy, computational efficiency, and robustness to varying data conditions, with the aim of determining which model provides the most reliable and effective predictions for the dataset generated through BO. The ML code was developed in Python 3 within the Jupyter Notebook environment, utilizing Python libraries such as NumPy and scikit-learn.[1 2 3]

[1] https://scikit-learn.org.
[2] https://numpy.org.
[3] https://jupyter.org.

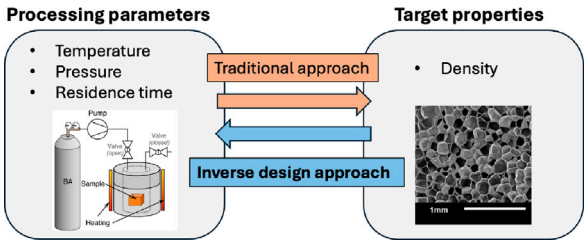

Fig. 2. Schematic representation of inverse design approach comparing to traditional approach in Autoclave batch foaming.

2.7. Inverse design

The goal of the inverse design technique is to identify a set of processing parameters that will yield a specific target density, a schematic representation can be seen in Fig. 2. The process involves deploying a model that relates the processing parameters to the resulting foam density and then using optimization techniques to find the parameters that produce the desired density. Let the desired foam density be denoted by ρ_{desired}. The foam density ρ can be expressed as a function of different processing parameters such as temperature T, pressure P, and saturation time t_s. Mathematically, the relationship can be represented as:

$$\rho = f(T, P, t_s) \tag{6}$$

The inverse design problem aims to find the optimal set of parameters T^*, P^*, t_s^* that result in the foam density ρ_{desired}. This can be formulated as an optimization problem:

$$\min_{T,P,t_s} \left| f(T, P, t_s) - \rho_{\text{desired}} \right| \tag{7}$$

The objective is to minimize the absolute difference between the predicted foam density and the target density. To solve this optimization problem, an iterative algorithm such as BO can be employed. The algorithm explores the parameter space and suggests new parameter sets likely to produce densities closer to the target. After obtaining the optimal parameters T^*, P^*, t_s^*, the final step is to verify the results experimentally. The foaming process is conducted under these conditions, and the resulting density is measured to confirm that it meets the desired target.

For example, in order to get the desired density ρ_{desired} of 50 kg/m^3, with the function $f(T, P, t_s)$ approximated using a Gaussian Process model, the inverse design problem involves iteratively adjusting the temperature, pressure, and saturation time until the foam density converges to approximately 50 kg/m^3. Note that during BO, all parameters are varied simultaneously, with each new suggested experiment consisting of three different values for temperature, pressure, and residence time. The workflow of the inverse design is as follows:

1. Identify the optimal processing parameters T, P, t_s to achieve the desired PA 12 foam density (ρ_{desired}).
2. Model the relationship between the processing parameters and PA 12 foam density.
3. Formulate and solve the optimization problem to minimize the difference between predicted and target densities.
4. Use Bayesian Optimization, an iterative algorithm, to refine the parameters.
5. Experimentally verify the results to confirm the desired PA 12 density is achieved.

3. Results and discussion

The primary goal of employing BO is to efficiently achieve low-density PA 12 foams during the autoclave batch foaming process. This approach not only aims to optimize the material properties with minimal experimental trials but also to generate a high-quality dataset for training an ML predictive model. By generating a comprehensive set of 1 million (10^6) virtual experiments, a parameter space encompassing various temperature, pressure, and time combinations was mapped out.

When optimizing a process like autoclave batch foaming to achieve low-density foam, one key step is to identify regions in the three-dimensional space of processing parameters, such as temperature, pressure, and saturation time, where the foam density reaches a high value, by keeping the density of the neat material as the reference. Understanding these regions allows us to define the "window" which is the range of parameters that will yield the low-density foam desired for optimization goals. By exploring the high-density regions in the three-dimensional space of T, P, and t_s, the range of parameters that helps avoid such outcomes can be defined. BO, with its posterior distribution, helps narrow the search to the most promising subspaces for achieving low-density foam.

To initiate the optimization process, the approach began with five random formulations. These included BO rounds, represented by blue triangles, aimed at maximizing each property; see Fig. 6. Remarkably, after just the first or second BO rounds, the suggested parameters demonstrated superior properties compared to all four initial random points. The optimization process also included Random (red circle) and AL (green square) rounds interspersed between the BO rounds. As anticipated, the BO rounds consistently resulted in higher property values than those achieved through the Random and AL approaches. Extending BO to explore a broader range of the parameter space successfully identified a plateau in the high-density region. This indicates that the optimization function is effectively navigating the three-dimensional space to pinpoint areas of maximum values in the space, as illustrated in Fig. 6. The trend toward this maximum plateau not only validates optimization strategy but also demonstrates the precision of the acquisition function in enhancing the desired property as needed.

Although the ultimate objective is to minimize density, understanding and achieving this high-density plateau allows us to rigorously test the BO framework. With this insight, the optimization process can be directed toward lower-density regions, paving the way for the development of low-density PA 12 batch foams. This optimization function highlights its versatility and potential for both maximizing and minimizing target properties as needed. To study the process-property relationship between bead density and other processing parameters, a correlation analysis was conducted. The correlation matrix, shown in Fig. 3 represents the relationships between key process parameters, including pressure, temperature, residence time, and the resulting density during PA 12 batch foaming. Seaborn's PairGrid was utilized to visualize these pairwise relationships, and Pearson correlation coefficients (denoted as R values) are displayed within Fig. 3. The full Pearson correlation figure is provided in the supporting information. To further investigate the relationships among these variables, a linear correlation analysis was conducted. The results revealed no strong linear correlation between the processing parameters. Therefore, quadratic, cubic, and fourth-order fits were explored to better capture potential non-linear relationships, with these additional analyses included in the supporting information.

In this correlation analysis, the main property, density, is compared with the process parameters: pressure, temperature, and saturation or residence time. The diagram provides insights into two-dimensional correlations without hiding information or leading to misinterpretations. Since no significant correlations exist among the processing parameters themselves, these plots will not be further elaborated. However, density is clearly influenced by the processing parameters, as shown at the bottom of Fig. 3 where density is plotted against pressure for all data points. It is evident that low densities are achieved at both low and high pressures. However, the trend line indicates that, in general, higher pressures lead to lower densities. This trend is consistent with observations in other studies [43,44], although it also depends

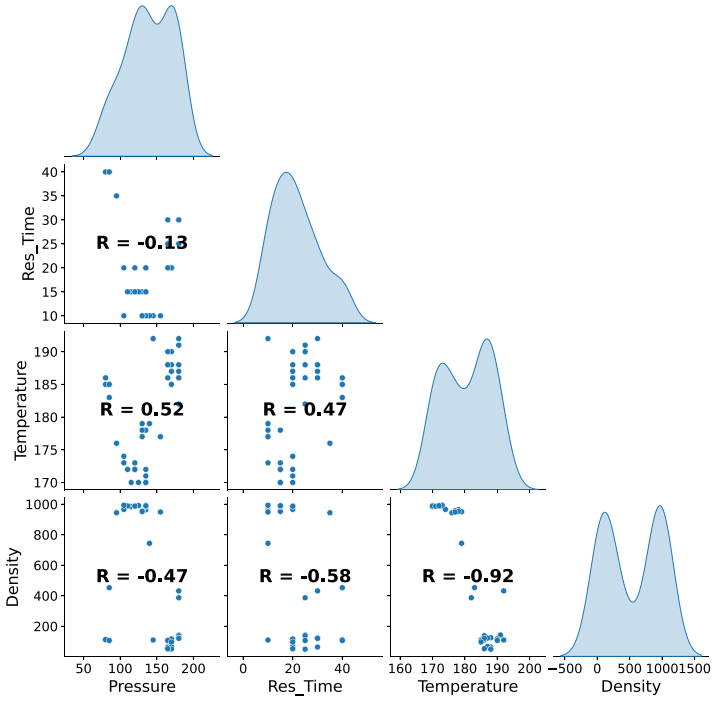

Fig. 3. A pairwise correlation plot showing the relationships between key variables (processing parameters) in the autoclave batch foaming of PA 12, where the **R** shows Pearson correlation coefficients.

on the selected temperature. The plot of temperature versus pressure shows that samples with low density and low pressure were processed at high temperatures, while samples with high density at medium pressure were processed at lower temperatures. These results highlight the interplay between selected pressure and temperature. When comparing density to residence time, no discernible trends are observed. Low and high densities are achieved at both extremes of residence time. Temperature, a well-known parameter for foaming, exhibits a negative correlation with density in this study. High temperatures generally lead to lower densities, as low temperatures restrict foaming, while sufficiently high temperatures enable it. However, previous studies [45, 46] often describe a local maximum, indicating that excessively high temperatures can hinder achieving lower densities. This relationship is further illustrated in the parallel coordinates plot Fig. 4, which shows the interactions between pressure, residence time, temperature, and density. The color gradient represents density, ranging from 50 (teal) to 1000 (rose). The overview of the ML model's performance on both the test and train sets can be seen in Fig. 5.

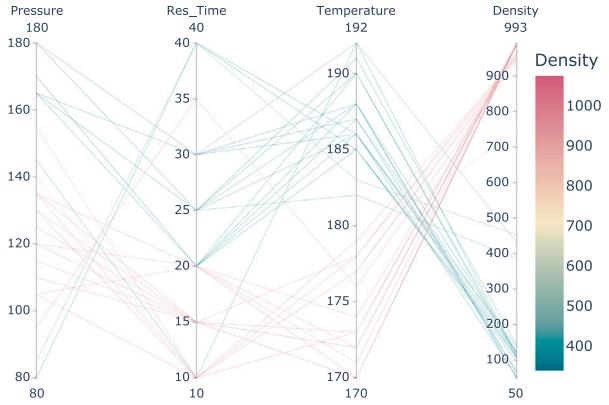

Fig. 4. Parallel coordinate plot showing the relationship between Pressure, Residence time, Temperature and density, for different combination of processing parameters in the batch foaming of PA 12 in Autoclave. (For interpretation of the references to color in this figure legend, the reader is referred to the web version of this article.)

3.1. Minimizing foam density

To achieve low-density PA 12 batch foam, previously measured data points situated in the high-density range were used as the starting point. The variation in density across a series of autoclave experiments is shown in Table 2. These points were chosen because they had been experimentally validated in the lab as having high density. Subsequently, BO was employed to systematically guide the optimization process toward developing low-density foam. In the BO process, a GP model was utilized as the regressor, paired with the maximum expected improvement acquisition function. This acquisition function effectively balanced exploitation (favoring low predicted values) and exploration (favoring high uncertainty). The GP model was constructed using three input variables: pressure, temperature, and residence time, with the aim of predicting density and its associated uncertainty. The Matérn kernel was employed within the GP model to enhance its flexibility and performance. Additionally, an AL strategy was integrated to propose uncorrelated processing parameters, further refining and enhancing the GP model in subsequent iterations.

In the first optimization trial, five new experimental suggestions were received. As shown in the first five rows of Table 2, the optimization process is proving effective, with a clear downward trend in density. The average density of these initial five experiments, after execution and measurement, is 187.5 kg/m^3, with a maximum density of 387 kg/m^3 (suggested AL point) and a minimum of 123 kg/m^3. This downward trend is visually represented in Fig. 7, demonstrating a successful transition into the low-density region. The dataset was progressively expanded with BO-suggested experiments until the minimum density target of 50 kg/m^3 was achieved. After multiple iterations, the optimization yielded densities as low as 51 kg/m^3, 56 kg/m^3, and 50 kg/m^3. These results confirm the establishment of a plateau in the low-density region for PA 12, as illustrated in Fig. 7. The best parameter combination for these densities was identified as a pressure of 170 bar, a temperature range of 187 °C–188 °C, and a residence time of 20 min.

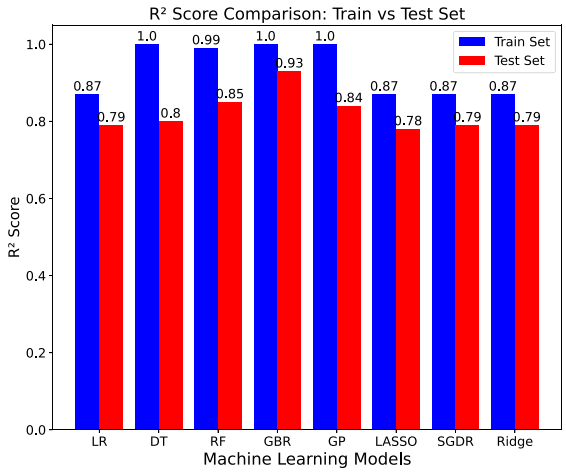

Fig. 5. R^2 score of each machine learning model used to predict the density for both train and test set. The dataset was generated from experimental trials following Bayesian optimization.

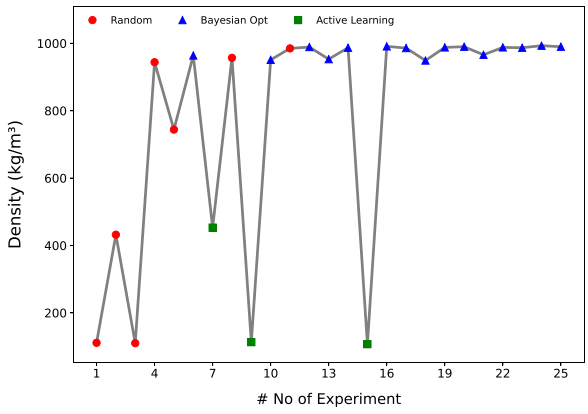

Fig. 6. Exploration of maximum value region. Evolution of Bayesian Optimization (blue triangles), Active Learning (green squares), and Random (red circles) techniques in optimizing the target property across a series of experiments. x-axis represent the experiment number, and the target property value on y-axis. (For interpretation of the references to color in this figure legend, the reader is referred to the web version of this article.)

Notably, the parameter space for the low density PA 12 batch foaming in the autoclave is quite narrow. Achieving low-density PA 12 beads requires maintaining the temperature within a narrow range of 185 °C to 192.5 °C. As highlighted by the correlation study (Fig. 3) and parameter combinations leading to density (Fig. 4), temperature is highly correlated with density. While pressure also influences density, its variation is broader, allowing for multiple effective combinations. Although the BO investigation reported in this study was highly efficient, it is important to note that there is no guarantee BO will consistently outperform initial random trials, even after multiple BO rounds. If BO runs do not perform as expected, alternative strategies, such as active learning experiments (e.g., uncertainty sampling) or additional random experiments, can be employed to enhance the GP model and potentially achieve convergence during BO runs. Exploring different kernels for the GP model or employing alternative acquisition functions in the BO procedure are additional strategies to improve suboptimal BO runs. However, if the selected features (parameters) are not intrinsically correlated with the target property, BO is unlikely to succeed regardless of the strategy used. The current hyperparameters used in the BO runs – such as the maximum expected improvement acquisition function and the RBF or Matérn kernel – have already proven effective, enabling a highly efficient optimization process. Notably, the density decreased

Table 2
Overview of Bayesian optimization suggested trials to minimize the density, where P = Pressure, R = Residence time, T = Temperature, and ED = Experimental Density.

Trials	P/bar	R/min	T/°C	ED/kg m^{-3}
1	180	25	191	143
2	180	30	188	125
3	180	25	186	138
4	180	25	182	387
5	180	30	187	123
6	180	30	186	121
7	180	25	189	117
8	80	30	186	110
9	145	30	192	110
10	170	25	188	64
11	170	20	190	68
12	165	30	188	107
13	170	20	187	51
14	165	25	190	97
15	170	20	188	50
16	170	25	186	53

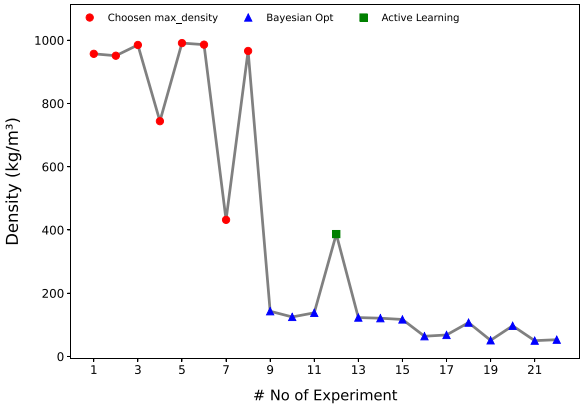

Fig. 7. Minimizing the density. Evolution of Bayesian Optimization (blue triangles), Active Learning (green squares), and Random (red circles) techniques in optimizing the target property across a series of experiments. On x-axis the experiment number, and y-axis represents the density. (For interpretation of the references to color in this figure legend, the reader is referred to the web version of this article.)

from approximately 900 kg/m^3 to 150 kg/m^3 within a single BO suggestion, as shown in Fig. 7. For further details on hyperparameter selection and optimization strategies, refer to a recent publication by the group [47], which provides an in-depth discussion of these topics.

3.2. Inverse design to achieve desired density

Using an inverse design approach, a model was developed to recommend optimal processing parameters for achieving specific bead densities. This method enabled efficient targeting and fine-tuning of density outcomes. Seven trials were conducted, each targeting different density values (referred to as the desired targets), with the results summarized in Table 3. The process demonstrates the model's ability to predict the processing parameters required to achieve precise densities. As seen in Table 3, the model performs particularly well for lower-density targets, with a low standard deviation. This consistency may be attributed to the model's prior exposure to data from the lower-density region. Further analysis of the inverse design revealed that for some density targets, the model suggests multiple combinations of processing parameters that yield approximately the same density. For example, a desired density of 110 kg/m^3 was achieved with different combinations of pressure (e.g., 80 bars and 145 bars) and temperature (e.g., 186 °C and 192 °C), while maintaining the same residence time. See Fig. 8 for the experimental density and desired density (or predicted density) .

To gain deeper insights, a density range of 70–80 kg/m^3 was selected as the target, and the inverse design provided approximately 90

Table 3
Overview of the inverse design trials, where *ED* = experimental density, and *DD* = desired (or predicted) density suggested from the inverse design. *P*, *R* and *T* are defined in the caption of Table 2.

Trials	*P*/bar	*R*/min	*T*/°C	DD (kg/m^3)	*ED*/kg m^{-3}
1	120	15	188	50	63
2	155	20	187	51	56
3	160	40	188	75	77
4	165	35	185	76	85
5	80	40	188	100	97.6
6	80	35	190	150	135
7	80	10	192	125	130

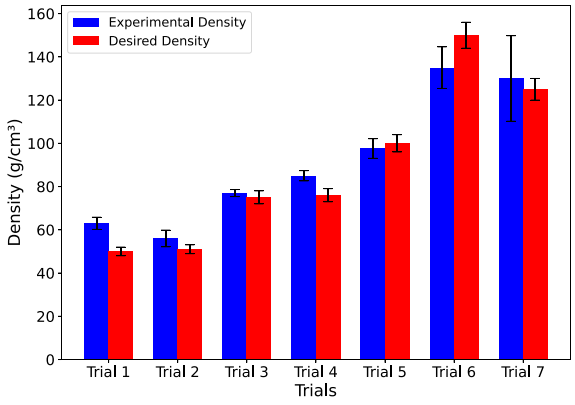

Fig. 8. The comparison of predicted and experimental densities of PA-12 bead foams for inverse design.

different parameter combinations. Four of these combinations were selected for experimental validation. The chosen parameters were based on an understanding of the autoclave process, allowing investigation of specific relationships between pressure, temperature, and residence time. For two trials, temperature and residence time were kept constant while varying the pressure from 80 to 180 bars. For the other two, a pressure of 140 bars was maintained with a residence time of 30 min, while the temperature was varied between 187.5 °C and 190 °C. These experiments provided clearer insights into how pressure and temperature affect the foaming behavior of PA 12 and demonstrated the robustness of the inverse design model in predicting processing parameters for different density targets.

3.3. Cell morphology

The properties of cellular materials like polymer foams are mainly influenced by both density and morphology. Factors like cell shape, size distribution, and structure of cell walls can lead to different properties, thus satisfying requirements for special applications. By utilizing the previously validated ML model, 90 individual parameter sets were generated out of the total 1 million possible virtual experiments, with predicted densities ranging from 70 kg/m^3 to 80 kg/m^3. To investigate the maximum spectrum of possible morphology, parameter sets were specifically selected from a pressure range of 80 bar to 180 bar, in combination with varying temperatures from 187.5 °C to 190.0 °C. The small possible variation in temperature, compared to the pressure, again indicates the high sensitivity of the autoclave process to that parameter. Residence time was kept constant at 30 min to ensure a state of equilibrium blowing agent sorption. The resulting cross-section of the foams via SEM can be seen in Fig. 9, supported by the resulting cell size distribution graph on the right side. Note that the trained ML model was simply used to suggest new low-density foams, whose cellular structures were later characterized and discussed. This model cannot predict cellular structures.

In general a clear trend is visible by comparing the morphology of the first three foamed samples. With higher pressures at similar temperatures, the average cell size gets smaller and cell density is increased while simultaneously narrowing its distribution. At 180 bar, a fine morphology of cell sizes around 31 μm was achieved Table 4. This behavior is directly linked to the increased pressure drop rate initiated by the higher saturation pressures [40]. This is also because a higher amount of CO_2 leads to higher pressure, which results in higher solubility, and as a result, a high number of nuclei form due to pressure drop and concentration. Thus, leading to a more pronounced thermodynamic disequilibrium between the polymer and the diluted blowing agent trying to separate throughout this process. In the initial state of the foaming process, this disequilibrium leads to the formation of nuclei within the system, which subsequently grow due to constant diffusion of the blowing agent from surrounding areas. This nucleation step was further investigated by calculating the density-corrected nucleation density. Here, a similar correlation is visible, with increasing nucleation density for higher saturation pressures. Finally, the parameter was set again at 140 bar, but with a slightly elevated temperature of 190.0 °C instead of 187.5 °C. Despite showing similar average cell sizes around 45 to 48 μm, the distribution appears to be more irregular. This can be attributed to the reduced viscosity of the polymer matrix at the elevated temperature, which can lead to a more unstable growth of the cells and possible coalescence by partial rupture of cell walls during expansion. Thus, indicating that foaming at lower temperatures around 188 °C results in a more stable and controllable process for precisely adjusting the foam morphology. In general, this chapter highlights the potential of the generated ML model to expand to further target parameters exceeding the currently used prediction of density. Within a small number of experiments, it is possible to generate virtual parameter sets for a defined density.

4. Conclusions

This study demonstrates the successful use of Bayesian Optimization (BO) and inverse design to optimize processing parameters for producing low-density PA 12 foams through autoclave batch foaming. By mapping a three-dimensional parameter space of temperature, pressure, and residence time, key regions for minimizing foam density were identified. The inverse design model effectively predicted optimal combinations of processing parameters, which were validated through experimental trials, enabling the achievement of desired density targets with minimal experimental effort.

It was observed that temperature plays a critical role in controlling foam density, with a narrow low-density foaming range between 185 °C and 192.5 °C. Pressure also showed significant effects, allowing for the achievement of low densities at various pressure levels, highlighting the flexibility of the process. Furthermore, the study confirmed that residence time exhibited no strong correlation with density, while temperature was inversely correlated, consistent with existing literature. Through the use of advanced optimization techniques, the density of PA 12 foam was reduced to as low as 50 kg/m^3, with the best results achieved using a pressure of 170 bar, a temperature of 187 °C, and a residence time of 20 min. These findings contribute to a deeper understanding of the process-property relationships in batch foaming and establish a robust framework for further optimization of polymer foaming processes.

This work not only advances the capability to fine-tune foam densities but also sets the foundation for future research in applying machine learning and optimization strategies to enhance material properties in polymer processing.

Table 4
Overview of processing parameters for the bead foam which is been analyzed with SEM, and also can see the SEM analysis data, Processing parameters (PP), Foam density (FD), Predicted density (PD) Mean cell size (MCS), Area cell density (ACD), Volumetric cell density (VCD), Nucleation density (ND).

PP	*FD* (kg/m^3)	*PD* (kg/m^3)	*MCS* (μm)	*ACD* (cell/cm^2)	*VCD* (cell/cm^3)	*ND* (nuclei/cm^3)
80 bar, 188 °C, 30 min	85	77	171 ± 25.7	5.40 * 10^5	3.97 * 10^8	4.79 * 10^9
140 bar, 187.5 °C, 30 min	87	77	48 ± 8.14	2.04 * 10^7	9.21 * 10^{10}	1.09 * 10^{12}
180 bar, 188 °C, 30 min	73	70	31 ± 3.862	6.50 * 10^7	5.24 * 10^{11}	7.36 * 10^{12}
140 bar, 190 °C, 30 min	66	73	45 ± 7.90	2.80 * 10^7	1.48 * 10^{11}	2.30 * 10^{12}

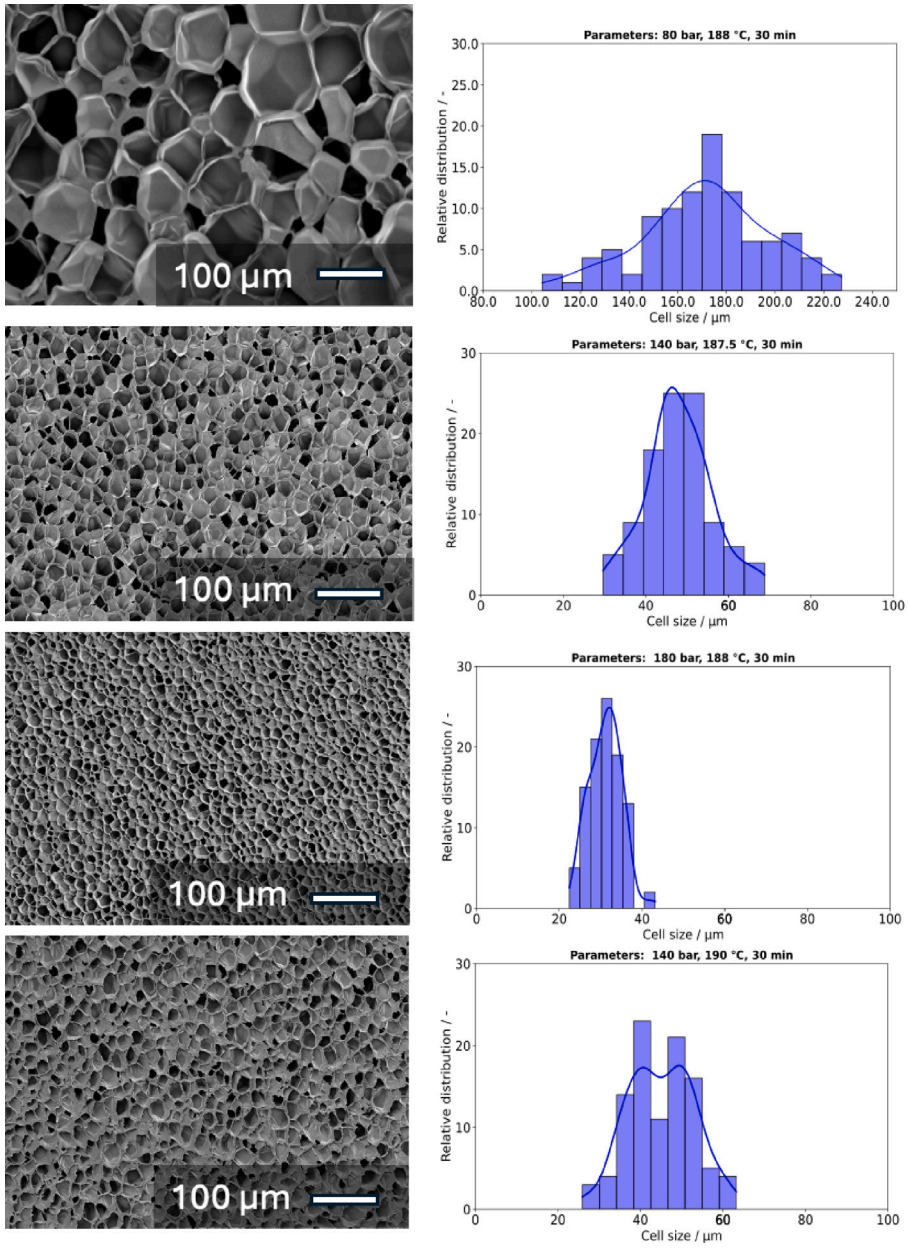

Fig. 9. Cell size distribution with the SEM images on the left size and respective data on the right size for different pressure and temperature.

CRediT authorship contribution statement

Karim Ali Shah: Writing – review & editing, Writing – original draft, Visualization, Validation, Methodology, Investigation, Formal analysis, Data curation, Conceptualization. **Rodrigo Q. Albuquerque:** Writing – review & editing, Validation, Supervision, Conceptualization. **Christian Brütting:** Writing – review & editing, Validation. **Marcel Dippold:** Writing – review & editing, Validation. **Holger Ruckdäschel:** Writing – review & editing, Project administration, Funding acquisition.

Declaration of competing interest

The authors declare that they have no known competing financial interests or personal relationships that could have appeared to influence the work reported in this paper.

Acknowledgments

The authors are thankful to the German Research Foundation (DFG) for funding this project with grant number *RU* 2586/5-1, project number *507656917*, and extend very sincere gratitude for the financial support provided. Special thanks to Evonik GmbH (Essen, Germany) for providing the materials used in this study. Thank you Annika Pfaffenberger for preparing the SEM pictures, the BPI KeyLab Electron and Optical Microscopy.

Appendix A. Supplementary data

The Python script (provided as a Jupyter notebook) is freely available on GitHub ("https://github.com/Polymer-Engineering-University-Bayreuth/BO").

Supplementary material related to this article can be found online at https://doi.org/10.1016/j.polymer.2025.128096.

Data availability

Data will be made available on request.

References

[1] Christian Brütting, Tobias Standau, Johannes Meuchelböck, Peter Schreier, Holger Ruckdäschel, A review on semi-crystalline polymer bead foams from stirring autoclave: Processing and properties, E- Polym. 23 (1) (2023) 20230092.
[2] Dorel Feldman, Polymer history, Des. Monomers Polym. 11 (1) (2008) 1–15.
[3] Hossein Abedsoltan, Applications of plastics in the automotive industry: Current trends and future perspectives, Polym. Eng. Sci. 64 (3) (2024) 929–950.
[4] Md Tanvir Hossain, Md Abdus Shahid, Nadim Mahmud, Ahasan Habib, Md Masud Rana, Shadman Ahmed Khan, Md Delwar Hossain, Research and application of polypropylene: a review, Discov. Nano 19 (1) (2024) 2.
[5] Mohammad Harun-Ur-Rashid, Abu Bin Imran, Md Abu Bin Hasan Susan, Green polymer nanocomposites in automotive and packaging industries, Curr. Pharm. Biotechnol. 24 (1) (2023) 145–163.
[6] Vaishali K Patel, Niketa Patel, Mittal D Patel, Hardik A Shukla, AlpeshKumar B Patel, Narendrasinh J Parmar, Innovations in lightweight materials for automotive engineering, J. Electr. Syst. 20 (10s) (2024) 2121–2133.
[7] Saul Utrera-Barrios, Raquel Verdejo, Miguel Ángel López-Manchado, Marianella Hernández Santana, Self-healing elastomers: A sustainable solution for automotive applications, Eur. Polym. J. 190 (2023) 112023.
[8] Amol C Bisen, Arpon Biswas, Ayush Dubey, Sachin N Sanap, Sristi Agrawal, Karan S Yadav, Vaishali Singh, Priyanka Rawat, Sudhanshu Sagar, Madhav N Mugale, et al., A review on polymers in ocular drug delivery systems, MedComm–Biomater. Appl. 3 (2) (2024) e77.
[9] Ketan Kuperkar, Leonard Ionut Atanase, Anita Bahadur, Ioana Cristina Crivei, Pratap Bahadur, Degradable polymeric bio (nano) materials and their biomedical applications: A comprehensive overview and recent updates, Polymers 16 (2) (2024) 206.
[10] Abul Kalam Azad, Joanne Lai, Wan Mohd Azizi Wan Sulaiman, Hassan Almoustafa, Salah Abdalrazak Alshehade, Vinoth Kumarasamy, Vetriselvan Subramaniyan, The fabrication of polymer-based curcumin-loaded formulation as a drug delivery system: an updated review from 2017 to the present, Pharmaceutics 16 (2) (2024) 160.
[11] Patrícia C Pires, Fouad Damiri, Ehsan Nazarzadeh Zare, Anwarul Hasan, Rasoul Esmaeely Neisiany, Francisco Veiga, Pooyan Makvandi, Ana Cláudia Paiva-Santos, A review on natural biopolymers in external drug delivery systems for wound healing and atopic dermatitis, Int. J. Biiol. Macromol. (2024) 130296.
[12] Md Enamul Hoque, Md Ushama Shafoyat, Fatiha Tabassun, Polymers, their composites, blends, and nanocomposites for the fabrication of prosthetics, Appl. Biopolym. Sci. Biotechnol. Eng. (2024) 361–389.
[13] Galina Satchanska, Slavena Davidova, Petar D. Petrov, Natural and synthetic polymers for biomedical and environmental applications, Polymers 16 (8) (2024) 1159.
[14] Teklebrahan Gebrekrstos Weldemhret, Yong Tae Park, Jung Il Song, Recent progress in surface engineering methods and advanced applications of flexible polymeric foams, Adv. Colloid Interface Sci. (2024) 103132.
[15] Márton Tomin, Ákos Kmetty, Polymer foams as advanced energy absorbing materials for sports applications—A review, J. Appl. Polym. Sci. 139 (9) (2022) 51714.
[16] Afeez Gbadamosi, Shirish Patil, Muhammad Shahzad Kamal, Ahmad A Adewunmi, Adeyinka S Yusuff, Augustine Agi, Jeffrey Oseh, Application of polymers for chemical enhanced oil recovery: a review, Polymers 14 (7) (2022) 1433.
[17] Junjie Jiang, Fang Liu, Bichi Chen, Yaozong Li, Xue Yang, Fangwei Tian, Donghua Xu, Wentao Zhai, Microstructure development of PEBA and its impact on autoclave foaming behavior and inter-bead bonding of EPEBA beads, Polymer 256 (2022) 125244.
[18] Justus Kuhnigk, Tobias Standau, Dominik Dörr, Christian Brütting, Volker Altstädt, Holger Ruckdäschel, Progress in the development of bead foams–a review, J. Cell. Plast. 58 (4) (2022) 707–735.
[19] Tobias Standau, Bianca Hadelt, Peter Schreier, Volker Altstadt, Development of a bead foam from an engineering polymer with addition of chain extender: Expanded polybutylene terephthalate, Ind. Eng. Chem. Res. 57 (50) (2018) 17170–17176.
[20] David Eaves, Handbook of Polymer Foams, iSmithers Rapra Publishing, 2004.
[21] Nemat Hossieny, Aboutaleb Ameli, Chul B. Park, Characterization of expanded polypropylene bead foams with modified steam-chest molding, Ind. Eng. Chem. Res. 52 (24) (2013) 8236–8247.
[22] Borja Muniz-Pardos, Shaun Sutehall, Konstantinos Angeloudis, Fergus M Guppy, Andrew Bosch, Yannis Pitsiladis, Recent improvements in marathon run times are likely technological, not physiological, Sports Med. 51 (3) (2021) 371–378.
[23] Wouter Hoogkamer, Shalaya Kipp, Jesse H Frank, Emily M Farina, Geng Luo, Rodger Kram, A comparison of the energetic cost of running in marathon racing shoes, Sports Med. 48 (4) (2018) 1009–1019.
[24] Zhaorui Xu, Guilong Wang, Jinchuan Zhao, Aimin Zhang, Guoqun Zhao, Super-elastic and structure-tunable poly (ether-block-amide) foams achieved by microcellular foaming, J. CO2 Util. 55 (2022) 101807.
[25] Dominik Dörr, Daniel Raps, Dharan Kirupanantham, Chris Holmes, Volker Altstädt, Expanded polyamide 12 bead foams (ePA) thermo-mechanical properties of molded parts, in: AIP Conference Proceedings, Vol. 2205, AIP Publishing, 2020.
[26] Sören Handtke, Lena Brömstrup, Jörg Hain, Fabian Fischer, Tim Ossowski, Sven Hartwig, Klaus Dröder, Investigation of recycled expanded polyamide beads through artificial ageing and mechanical recycling as a proof of concept for circular economy, Polymers 16 (12) (2024) 1730.
[27] DonHee Lee, Seong No Yoon, Application of artificial intelligence-based technologies in the healthcare industry: Opportunities and challenges, Int. J. Environ. Res. Public Health 18 (1) (2021) 271.
[28] Vijaya Kanaparthi, Transformational application of artificial intelligence and machine learning in financial technologies and financial services: A bibliometric review, 2024, arXiv preprint arXiv:2401.15710.
[29] Tahamina Nasrin, Farhad Pourkamali-Anaraki, Amy M. Peterson, Application of machine learning in polymer additive manufacturing: A review, J. Polym. Sci. 62 (12) (2024) 2639–2669.
[30] Sudarsan M. Pai, Karim A. Shah, Sruthi Sunder, Rodrigo Q. Albuquerque, Christian Brütting, Holger Ruckdäschel, Machine learning applied to the design and optimization of polymeric materials: A review, Next Mater. 7 (2025) 100449.
[31] Karim Ali Shah, Christian Brütting, Rodrigo Q Albuquerque, Holger Ruckdäschel, Machine learning investigation of polylactic acid bead foam extrusion, J. Appl. Polym. Sci. (2024) e55693.
[32] Melvin I Pech-Mendoza, Alejandro E Rodríguez-Sánchez, Héctor Plascencia-Mora, Neural networks-based modeling of compressive stress in expanded polystyrene foams: A focus on bead size parameters, Proc. Inst. Mech. Eng. Part L: J. Mater.: Des. Appl. (2024) 14644207231224172.
[33] Rodrigo Q Albuquerque, Christian Brütting, Tobias Standau, Holger Ruckdäschel, A machine learning investigation of low-density polylactide batch foams, E-Polym. 22 (1) (2022) 318–331.
[34] Karim Ali Shah, Rodrigo Q Albuquerque, Christian Brütting, Holger Ruckdäschel, Machine learning-based time series analysis of polylactic acid bead foam extrusion, J. Appl. Polym. Sci. (2024) e56170.
[35] Sirawit Pruksawan, Guillaume Lambard, Sadaki Samitsu, Keitaro Sodeyama, Masanobu Naito, Prediction and optimization of epoxy adhesive strength from a small dataset through active learning, Sci. Technol. Adv. Mater. 20 (1) (2019) 1010–1021.
[36] James R Deneault, Jorge Chang, Jay Myung, Daylond Hooper, Andrew Armstrong, Mark Pitt, Benji Maruyama, Toward autonomous additive manufacturing: Bayesian optimization on a 3D printer, MRS Bull. 46 (2021) 566–575.
[37] Kundo Park, Youngsoo Kim, Minki Kim, Chihyeon Song, Jinkyoo Park, Seunghwa Ryu, Designing staggered platelet composite structure with Gaussian process regression based Bayesian optimization, Compos. Sci. Technol. 220 (2022) 109254.
[38] Sterling G. Baird, Jason R. Hall, Taylor D. Sparks, Compactness matters: Improving Bayesian optimization efficiency of materials formulations through invariant search spaces, Comput. Mater. Sci. 224 (2023) 112134.
[39] Patrick Endres, Timo Schuett, Christian Brütting, Julian Kimmig, Rodrigo Q Albuquerque, Tobias Standau, Stefan Zechel, Holger Ruckdäschel, Ulrich S Schubert, Systematic copolymer screening for foaming experiments supported by computational methods, J. Mater. Chem. A 11 (47) (2023) 26183–26192.
[40] Marcel Dippold, Holger Ruckdäschel, Influence of pressure-induced temperature drop on the foaming behavior of amorphous polylactide (PLA) during autoclave foaming with supercritical CO2, J. Supercrit. Fluids 190 (2022) 105734.
[41] Christian Brütting, Julia Dreier, Christian Bonten, Holger Ruckdäschel, Biobased Immiscible Polylactic Acid (PLA): Poly (3-hydroxybutyrate-co-3-hydroxyvalerate)(PHBV) Blends: Impact of rheological and non-isothermal crystallization on the bead foaming behavior, J. Polym. Environ. (2024) 1–14.

[42] Rodrigo Q Albuquerque, Florian Rothenhäusler, Holger Ruckdäschel, Designing formulations of bio-based, multicomponent epoxy resin systems via machine learning, MRS Bull. 49 (1) (2024) 59–70.
[43] Marcelo Antunes, Vera Realinho, José Ignacio Velasco, Study of the influence of the pressure drop rate on the foaming behavior and dynamic-mechanical properties of co2 dissolution microcellular polypropylene foams, J. Cell. Plast. 46 (6) (2010) 551–571.
[44] Zhi Mei Xu, Xiu Lei Jiang, Tao Liu, Guo Hua Hu, Ling Zhao, Zhong Nan Zhu, Wei Kang Yuan, Foaming of polypropylene with supercritical carbon dioxide, J. Supercrit. Fluids 41 (2) (2007) 299–310.
[45] Yves Marie Corre, Abderrahim Maazouz, Jannick Duchet, Joël Reignier, Batch foaming of chain extended PLA with supercritical CO2: Influence of the rheological properties and the process parameters on the cellular structure, J. Supercrit. Fluids 58 (1) (2011) 177–188.
[46] Christian Brütting, Julia Dreier, Christian Bonten, Volker Altstädt, Holger Ruckdäschel, Sustainable Immiscible Polylactic Acid (PLA) and Poly(3-hydroxybutyrate- co -3-hydroxyvalerate) (PHBV) Blends: Crystallization and Foaming Behavior, ACS Sustain. Chem. Eng. 11 (17) (2023) 6676–6687.
[47] Florian Rothenhäusler, Holger Ruckdaeschel, Strategies for the fast optimization of the glass transition temperature of sustainable epoxy resin systems via machine learning, J. Appl. Polym. Sci. 141 (21) (2024) e55422.